Dynamic assembly of surface structures in living cells

Julia Gorelik*, Andrew I. Shevchuk*, Gregory I. Frolenkov†, Ivan A. Diakonov*, Max J. Lab*, Corné J. Kros‡, Guy P. Richardson‡, Igor Vodyanoy§, Christopher R. W. Edwards¶, David Klenerman‖, and Yuri E. Korchev*,**

*Division of Medicine, Imperial College London, Hammersmith Hospital Campus, Du Cane Road, London W12 0NN, United Kingdom; †National Institute on Deafness and Other Communication Disorders, National Institutes of Health, Bethesda, MD 20892-8027; ‡School of Biological Sciences, University of Sussex, Falmer, Brighton BN1 9QG, United Kingdom; §Office of Naval Research, Arlington, VA 22217; ¶Department of Physiological Sciences, University of Newcastle, Newcastle upon Tyne NE1 7RU, United Kingdom; and ‖Department of Chemistry, Cambridge University, Cambridge CB2 1EW, United Kingdom

Edited by Lewis G. Tilney, University of Pennsylvania, Philadephia, PA, and approved March 24, 2003 (received for review January 27, 2003)

Although the dynamics of cell membranes and associated structures is vital for cell function, little is known due to lack of suitable methods. We found, using scanning ion conductance microscopy, that microvilli, membrane projections supported by internal actin bundles, undergo a life cycle: fast height-dependent growth, relatively short steady state, and slow height-independent retraction. The microvilli can aggregate into relatively stable structures where the steady state is extended. We suggest that the intrinsic dynamics of microvilli, combined with their ability to make stable structures, allows them to act as elementary ''building blocks'' for the assembly of specialized structures on the cell surface.

Relatively short (<500-nm) microvilli are observed on the surfaces of most cells, including fibroblasts, growing neurons, and epithelial cells. As any microvilli, they are supported by a characteristic central core of parallel actin filaments densely packed with cross-linking actin-binding proteins (1–3). It is assumed that these short microvilli may develop into larger microvillar structures, like the intestinal brush border microvilli or the stereocilia of hair cells of the mammalian inner ear (4, 5). The large specialized microvilli in the intestine and inner ear were reported to be relatively stable throughout the life of the cell (6, 7). Although the cytoskeletal proteins in the core of these large microvilli undergo continuous turnover (8, 9), their relative stability is likely to be determined by a dynamic steady state (10, 11). In contrast, almost nothing is known about the stability of the shorter microvilli, even though they are the most abundant. This is due to the lack of suitable methods to quantitatively study microvillar dynamics.

Imaging of any subcellular structures with 10s of nanometers resolution, such as microvilli in a living cell, represents a technical challenge, because these dimensions cannot be reliably resolved with optical microscopy. Atomic force microscopy (AFM) could theoretically resolve even smaller objects in living cells (12), but substantial mechanical interaction between the specimen and the AFM probe makes it extremely difficult to image microvilli on the surface of living cells (13, 14). Scanning ion conductance microscopy (SICM) (15) does not apply mechanical force to the specimen, because it uses the ion current passing through the scanning pipette to derive the feedback signal. This technique enables noninvasive imaging of living cells (16, 17), including high-resolution imaging of microvilli (Fig. 1) (18–20). Here we have used SICM to observe directly the assembly of microvillar structures in various living epithelial and nonepithelial cells.

Materials and Methods

A6 Cell Preparation. A6 toad kidney epithelium cells (gift of P. DeSmet, Katholieke Universiteit, Leuven, Belgium) were cultured on membrane filters (Falcon) as described (21). Cell culture medium contained (per 1 liter) 375 ml of Leibovitz's L15 culture medium, 375 ml of Ham's F12 medium, 100 ml of FCS, 20 ml of L-glutamine, and 3 ml of 7.5% sodium bicarbonate (all solutions from GIBCO). This mixture gives final concentrations of 105 mM of NaCl and 25 mM of $NaHCO_3$. The medium was supplemented with 200 μg/ml streptomycin and 200 units/ml penicillin (GIBCO). All experiments were carried out between 127 and 134 passages. Cells were maintained at 28°C in an atmosphere of humidified air supplemented with 1% CO_2. Cells were used on the 4th to 5th days after placing in the culture, when they were 90–95% confluent. During the experiments, both sides of the epithelial layer were bathed with identical isoosmotic solution. This solution had an osmolality of 320 milliosmolar/kg, pH 7.4 and contained (in mM): 140 NaCl, 5 KCl, 0.8 $MgCl_2$, 1.2 $CaCl_2$, and 10 Hepes.

Organotypic Cultures of the Organ of Corti. The cultures were prepared from cochleas of 3-day-old mouse pups (Swiss CD-1, Charles River Breeding Laboratories) according to the procedure described (22), with some modifications. Briefly, strips of the organ of Corti were carefully microdissected and placed in Leibowitz cell culture medium, L-15 (GIBCO). Reissner's membrane and tectorial membrane were removed with fine forceps. Apical turn, middle turn, and apical half of the basal turn of the organ of Corti were separated, transferred to the DMEM/F12 medium supplemented with 7% FBS (GIBCO), and adhered to the bottom of the Petri dish coated with CellTak (Collaborative BioMedical Products, Bedford, MA). Cultures were maintained at 37°C and 5% CO_2 for 1–5 days before use. Immediately before the experiment, the medium was changed to L-15.

SICM Imaging. The basic arrangement of the SICM for topographical imaging of living cells has been described (18, 19). Briefly, the sensitive probe of the SICM is a glass micropipette (Fig. 1) filled with electrolyte, which is connected to a high-impedance head-stage current amplifier. The probe is mounted on a three-axis piezo translation stage toward the sample bathed in conductive medium. The control electronics use the ion current that flows through the tip of the micropipette as a feedback signal to move the stage up or down, to keep the probe-sample separation constant during X-Y scanning. Computer control acquires topographical data and generates a high-resolution image of the surface. The stability of imaging was greatly improved in our setup by a distance-modulated control (20) (at 1-kHz modulation frequency). The scanning pipettes were made from 1-mm outer and 0.58-mm inner diameter glass microcapillaries (Intracel, Herts, U.K.) using a laser-based Brown Flaming puller (model P-2000, Sutter Instruments, San Rafael, CA). The inner diameter of the micropipette was estimated by scanning electron microscopy (SEM) to be about 100 nm.

Sample Preparation for SEM. Well developed monolayers grown on either filters or glass coverslips were chosen for SEM. They were

This paper was submitted directly (Track II) to the PNAS office.

Abbreviations: SEM, scanning electron microscopy; SICM, scanning ion conductance microscopy.

**To whom correspondence should be addressed. E-mail: y.korchev@ic.ac.uk.

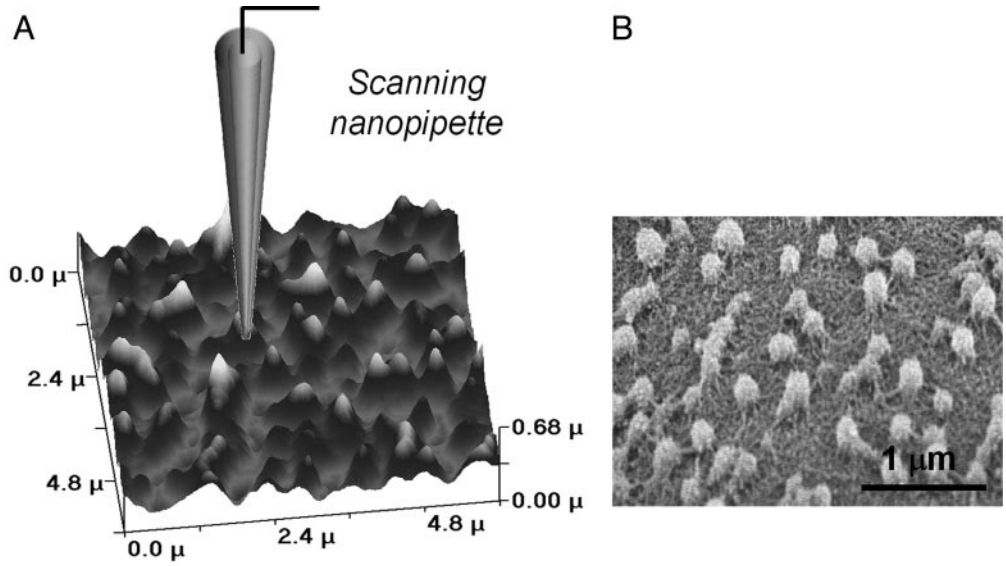

Fig. 1. SICM (*A*) and SEM (*B*) images of microvillar structures in *Xenopus* kidney epithelial A6 cells. (*A*) A SICM probe scanning the cell surface of an A6 cell. (*B*) A SEM image of a similar A6 cell. To reveal the cortical cytoskeleton, the plasma membrane was removed by a mild detergent. (Bar = 1 μm.)

fixed at room temperature (23°C) in 1% glutaraldehyde for 40 min and postfixed in 1% OsO_4 for 20 min. Dehydration was carried out with an ethanol series. The specimens were critical-point dried from liquid CO_2, sputter-coated with platinum, and observed with a field-emission scanning electron microscope.

Results and Discussion

Xenopus kidney epithelial A6 cells form a monolayer with well established tight junctions (Fig. 2*A*) and numerous microvillar structures (Fig. 1). These microvilli are supported by the bundles of actin filaments extending from the cortical cytoskeleton (Fig.

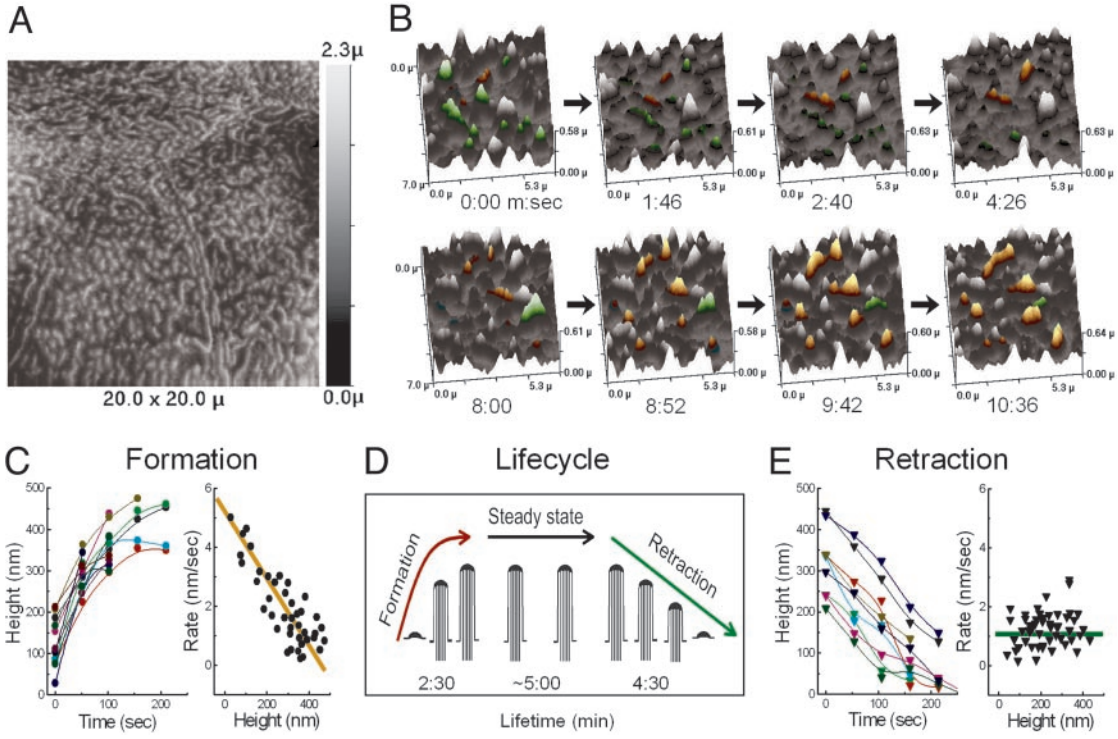

Fig. 2. Dynamics of individual microvilli in a living epithelial cell (A6 cell line). (*A*) Topographical SICM image of cells with well formed microvilli. (*B*) High-resolution time-lapse imaging of microvilli. Microvilli that are forming, retracting, or relatively ''stable'' are highlighted orange, green, and white, respectively. (*Upper*) Prevailing retraction of microvilli. (*Lower*) The same area at a later period, when the formation of microvilli prevails. Each image took 50 s to acquire. The complete sequence of images acquired in the experiment is presented as Movie 1, which is published as supporting information on the PNAS web site, www.pnas.org. (*C*) Heights of individual microvilli increase nonlinearly during their formation (*Left*); height-dependent rate of microvilli formation (n = 66) (*Right*). (*D*) Schematic diagram of the life cycle of microvilli: formation, steady state, and retraction. (*E*) Individual microvilli undergo linear decrease of height during retraction (*Left*). Height-independent rate of microvilli retraction (n = 59) (*Right*). The experiment was performed at 27°C

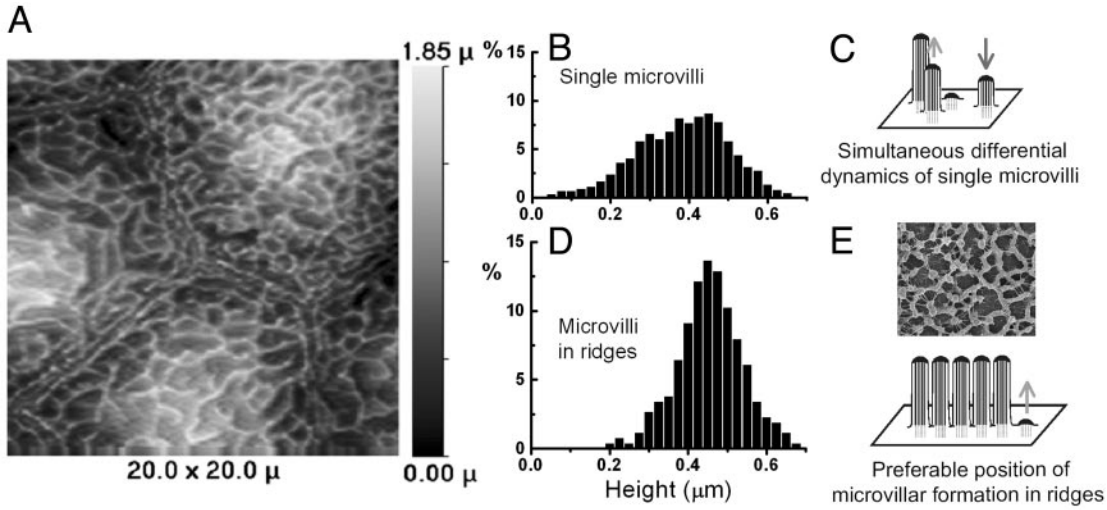

Fig. 3. Formation of ridges in living epithelial cell (A6 cell line). (*A*) Topographical SICM image of cells with well formed ridges. (*B*) The distribution of heights of single microvilli. (*C*) Schematic diagram of simultaneous formation and retraction of single neighboring microvilli. (*D*) The distribution of heights of microvilli in ridges. (*E*) SEM image showing individual microvilli arranged into the ridges (*Upper*). (Bar = 1 μm.) Schematic diagram of sidewise formation of microvilli in ridges (*Lower*).

1*B*). Time-lapse SICM imaging showed that these microvilli are dynamic structures (Fig. 2*B*). Even after 10 h of continuous observation, we have not noted any signs of slowing down of the microvillar dynamics. However, the addition of 1% formaldehyde to the bath medium effectively stopped any changes of microvillar shape (data not shown).

We observed that the microvillar density usually varied between different A6 cells within the same monolayer. By choosing a cell where the density of microvilli was low, allowing identification of individual microvilli, it was possible to quantify the dynamics of single microvilli (Fig. 2*B*). At any given time, some microvilli grew (marked orange), whereas the neighboring ones retracted (marked green). However, there was also a general tendency of the cell to retract (Fig. 2*B Upper*) or form (Fig. 2*B Lower*) microvilli at different periods of time. In the illustrated cell, the microvillar dynamics changed from retraction to formation during the 200 s separating the two sets of frames shown in Fig. 2*B Upper* and *Lower*. Often microvilli are formed along an axis (Fig. 2 *A* and *B*). Even those microvilli that did not grow or retract were not strictly "stable," showing some lateral rearrangement (Fig. 2).

Initially, microvilli grew at a rate of about 5 nm/s (Fig. 2*C*). As the microvillus increased in height, the rate of growth decreased, which eventually resulted in the cessation of their growth (Fig. 2*C*). In contrast, the retraction of microvilli occurred at a rate of about 1.2 nm/s, which remained constant and independent on the microvilli height (Fig. 2*E*). The observed life cycle of a microvillus is depicted in Fig. 2*D*. After a short period of rapid growth, which characterizes a sudden appearance of a microvillus, a steady state ensues, followed by a retraction at a constant rate. An average duration of this cycle was found to be 12.1 $\pm$ 5.6 min (n = 244).

Formation of multiple aggregates of microvilli often led to ridge-like structures. Almost 50% of the cells in the monolayer had ridges rather than individual microvilli (Fig. 3*A*). It could be observed that the assembly of a ridge was initiated by the formation of a new microvillus alongside an existing one. Then the neighboring microvilli contact each other, forming relatively stable aggregates (Fig. 3*E*). Newly formed microvilli never associate together as a clump. They could associate only laterally to form a ridge. Sometimes these ridges angled at precisely 120°. The ridges had a unique height (within the boundaries of the normal distribution), whereas individual microvilli had a population of shorter microvilli (Fig. 3 *B* and *D*), which may reflect their formation or retraction (Fig. 3*C*).

To validate that the observed microvillus dynamics is not a specific property of a cultured cell line but rather a wide-ranging cellular phenomenon, we studied the microvillar dynamics in different cell types (including human cells). One example is epithelial nonsensory cells of the mouse organ of Corti. The well developed short microvilli of these cells could be considered predecessors of the stereocilia of sensory hair cells (5). In organotypic culture conditions (22), these epithelial supporting cells still possess a microvillar coating, albeit not as dense as *in*

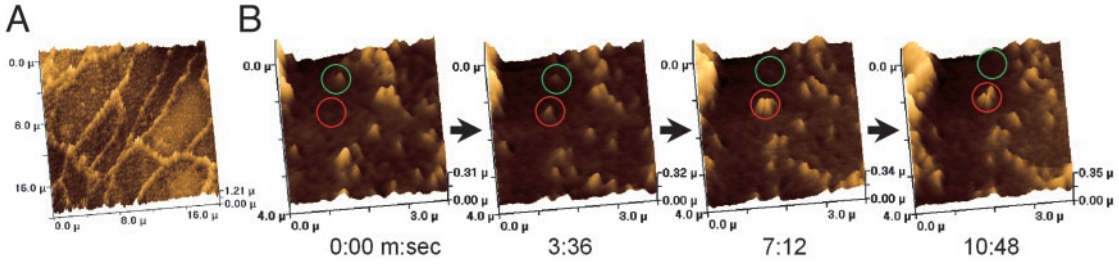

Fig. 4. Microvillar dynamics in the epithelial cells of the mouse organ of Corti. (*A*) SICM image of Hensen's cells in a 3-day-old organotypic cochlear culture. (*B*) Time-lapse sequence of four images of a smaller area close to border of one of the cells shown in *A*. Green and red circles point to retracting and forming microvilli, respectively. Temperature of the bathing L-15 medium was 27°C.

vivo (23). One type, Hensen's cells, is shown in Fig. 4*A*. Similar to A6 cells, time-lapse SICM observations revealed ongoing dynamics of microvilli on the surface of these Hensen's cells (Fig. 4*B*). Remarkably, the rates of microvilli formation and retraction in these mammalian epithelial cells were similar to those of the *Xenopus* A6 cells. In the example shown in Fig. 4*B*, it took about 3 min for the microvillus to form, which is very close to the values measured for A6 cells (Fig. 2*C*). Similar to A6 cells, the retraction of microvilli was slower. Analogous microvillar dynamics was also observed in another type of epithelial supporting cells of the organ of Corti, outer phalangeal cells (data not shown). As expected, the larger microvillar structures, stereocilia of sensory hair cells, were substantially more stable, showing no signs of dynamic changes of height or lateral arrangement within the accuracy of SICM imaging technique (data not shown). In addition, we performed time-lapse imaging of the surface of the following cell types: human colon cancer cells (CACO-2 line), murine melanocytes (melan-b line), breast cancer cells (T47D cell line), and fibroblasts (COS-7 cell line) (data not shown). In all these cells, we observed microvillar dynamics similar to those described above. We think, therefore, that these microvillar dynamics are likely to be a common phenomenon for short nonspecialized microvilli irrespective of their cell origin.

Several features of this dynamics should be noted. The initial formation rate of individual microvilli is about 5 nm/s, which is very close to the rate of elongation of the fertilization cone in sea urchin egg (5.5 nm/s) (24) and three to six times less than typical rates of filopodium extension (15–30 nm/s) (25). This is unlikely to be a simple coincidence. In contrast to filopodia, parallel actin fibers in microvilli and the fertilization cone are densely packed into bundles by different cross-linking proteins (26). The measured initial formation rate of these structures probably reflects the speed of assembly of the whole bundle. The rate of growth in our experiments shows a distinct inverse relationship with the height of the microvillus (Fig. 2*C*). This would be expected if formation of the microvillus depends on simple diffusion of actin and actin-binding proteins to its tip. As the microvillus grows, the longer diffusion path leads to a decrease in the rate of actin bundle assembly. A microvillus stops growing when the rate of formation becomes equal to the rate of ongoing actin depolymerization. Such dynamic steady-state equilibrium between actin bundle formation and actin depolymerization was proposed to regulate the length of large microvillar structures like *Drosophila* bristles (7), brush border microvilli (11), or stereocilia of hair cells (10). In our experiments, microvilli after formation were in a steady state for $\approx$5 min, followed by retraction with a constant rate of 1.2 nm/s (Fig. 2*E*), which is much slower than formation rate and is comparable to the rate of actin depolymerization at 2 nm/s (27). These data suggest that, at least in the retraction phase, actin polymerization is blocked and not involved in the control of the microvillar height. However, it is not clear what signal controls retraction or growth of a microvillus. Presumably this on/off signal has to operate locally, because two neighboring microvilli may exist in different phases of their life cycle (Fig. 3*C*).

It has been proposed that microvilli serve as "the archetypal factory of an actin bundle" (26), constantly providing a cell with organized bundle assemblies, which could be used by the cell to form larger specialized microvillar structures. Here we have shown that microvilli are constantly changing, which indeed implies ongoing assembly and disassembly or utilization of actin bundles. In fact, the dynamics of actin assembly in cortical cytoskeleton (28) is strikingly similar to the microvillar dynamics observed in our experiments. Moreover, microvillar dynamics also provide clusters of microvilli, which serve as crystallization points for more stable surface structures, where the microvillar steady state is prolonged. Therefore, we conclude that microvilli may serve as elementary "building blocks" of the larger structures on the surface of the cell.

This work was supported by the Biotechnology and Biological Science Research Council, the Office of Naval Research, and the Wellcome Trust.

1. Tilney, L. G. & Mooseker, M. (1971) *Proc. Natl. Acad. Sci. USA* **68,** 2611–2615.
2. Ezzell, R. M., Chafel, M. M. & Matsudaira, P. T. (1989) *Development (Cambridge, U.K.)* **106,** 407–419.
3. Bartles, J. R., Zheng, L., Li, A., Wierda, A. & Chen, B. (1998) *J. Cell Biol.* **143,** 107–119.
4. Chambers, C. & Grey, R. D. (1979) *Cell Tissue Res.* **204,** 387–405.
5. Sobin, A. & Anniko, M. (1984) *Arch. Otorhinolaryngol.* **241,** 55–64.
6. Stidwill, R. P.& Burgess, D. R. (1986) *Dev. Biol.* **114,** 381–388.
7. Guild, G. M., Connelly, P. S., Vranich, K. A., Shaw, M. K. & Tilney, L. G. (2002) *J. Cell Sci.* **115,** 641–653.
8. Lecount, T. S. & Grey, R. D. (1972) *J. Cell Biol.* **53,** 601–605.
9. Stidwill, R. P., Wysolmerski, T. & Burgess, D. R. (1984) *J. Cell Biol.* **98,** 641–645.
10. Schneider, M. E., Belyantseva, I. A., Azevedo, R. B. & Kachar, B. (2002) *Nature* **418,** 837–838.
11. Tyska, M. J. & Mooseker, M. S. (2002) *Biophys. J.* **82,** 1869–1883.
12. Le Grimellec, C., Lesniewska, E., Giocondi, M. C., Finot, E., Vie, V. & Goudonnet, J. P. (1998) *Biophys. J.* **75,** 695–703.
13. Braet, F., Seynaeve, C., De Zanger, R. & Wisse, E. (1998) *J. Microsc.* **190,** 328–338.
14. Lesniewska, E., Giocondi, M. C., Vie, V., Finot, E., Goudonnet, J. P. & Le Grimellec, C. (1998) *Kidney Int. Suppl.* **65,** S42–S48.
15. Hansma, P. K., Drake, B., Marti, O., Gould, S. A. & Prater, C. B. (1989) *Science* **243,** 641–643.
16. Gu, Y., Gorelik, J., Spohr, H. A., Shevchuk, A., Lab, M. J., Harding, S. E., Vodyanoy, I., Klenerman, D. & Korchev, Y. E. (2002) *FASEB J.* **16,** 748–750.
17. Korchev, Y. E., Negulyaev, Y. A., Edwards, C. R. W., Vodyanoy, I. & Lab, M. J. (2000) *Nat. Cell Biol.* **2,** 616–619.
18. Korchev, Y. E., Milovanovic, M., Bashford, C. L., Bennett, D. C., Sviderskaya, E. V., Vodyanoy, I. & Lab, M. J. (1997) *J. Microsc.* **188,** 17–23.
19. Korchev, Y. E., Bashford, C. L., Milovanovic, M., Vodyanoy, I. & Lab, M. J. (1997) *Biophys. J.* **73,** 653–658.
20. Shevchuk, A. I., Gorelik, J., Harding, S. E., Lab, M. J., Klenerman, D. & Korchev, Y. E. (2001) *Biophys. J.* **81,** 1759–1764.
21. Sariban-Sohraby, S., Burg, M. B. & Turner, R. J. (1984) *J. Biol. Chem.* **259,** 11221–11225.
22. Russell, I. J. & Richardson, G. P. (1987) *Hear. Res*, **31,** 9–24.
23. Furness, D. N., Richardson, G. P. & Russell, I. J. (1989) *Hear. Res.* **38,** 95–109.
24. Begg, D. A., Rebhun, L. I. & Hyatt, H. (1982) *J. Cell Biol.* **93,** 24–32.
25. Mallavarapu, A. & Mitchison, T. (1999) *J. Cell Biol.* **146,** 1097–1106.
26. DeRosier, D. J. & Tilney, L. G. (2000) *J. Cell Biol.* **148,** 1–6.
27. Pollard, T. D., Blanchoin, L. & Mullins, R. D. (2000) *Annu. Rev. Biophys. Biomol. Struct.* **29,** 545–576.
28. Schafer, D. A., Welch, M. D., Machesky, L. M., Bridgman, P. C., Meyer, S. M. & Cooper, J. A. (1998) *J. Cell Biol.* **143,** 1919–1930.